Effect of unresolved structures on the Euler-Euler simulation of 3D periodic circulating fluidized of binary mixture

Effect of unresolved structures on the Euler-Euler simulation of 3D periodic circulating fluidized of binary mixture

A. Ozel*,†, P. Fede*,† and O. Simonin*,†

* Université de Toulouse; INPT, UPS; IMFT; 31400 Toulouse, France

† CNRS; Institut de Mécanique des Fluides de Toulouse; 31400 Toulouse, France

pascal.fede@imft.fr and olivier.simonin@imft.fr

Keywords: Two-fluid model, Fluidized bed, LES approach

Abstract

It is well established that small-scale structures have an important effect on the overall hydrodynamic behaviour of dense and circulating fluidized bed. Due to computational constraints, the numerical simulations of practical applications with Euler-Euler two-phase approach are usually performed with relatively coarse mesh with respect to the local segregation of solid. These simulations cancel out the small-scale solid structures. All previous studied attempted to take into account the effect of unresolved structures on the drag force in the case where the particulate phase is monodisperse. This paper is dedicated to analyse the unresolved structures effects on polydisperse gas-solid flow by multi-fluid Eulerian approach. In this study, the binary mixture is conducted by gas at an ambient condition in a 3D periodic circulating fluidized bed. The aim is first to obtain mesh independent results where further mesh refinement is not necessary. Then these results are used to investigate the unresolved structures effects on resolved field by following *a priori* methodology. In particular, the role of small-scale structures on the momentum transfer by inter-particle collisions is pointed out.

INTRODUCTION

Even if the efficiency of computers is still increasing the Euler-Euler numerical simulations of industrial processes such as fluidized polymerization reactor, fluidized cracking column or coal fluidized boiler are frequently performed with grids too coarse to allow the accurate prediction of the local segregation effects. In particular, for a given type of particles (A-type or A/B-type according to Geldart's classification) several studies have shown that the cell-size must be of the order of few particle diameters to predict accurately the dynamical behavior of a fluidized bed (Agrawal et al., 2001; Heynderickx et al., 2004). Indeed, it has been shown that small-scale solid structures play a drastic effect on the fluid-particle momentum transfer mechanisms. Therefore, neglecting such solid structures leads to an overestimation of the predicted drag and consequently to an overestimation of the bed height for dense fluidized bed and an overestimation of the solid mass flux entrainment in circulating fluidized bed.

In a similar manner to LES approach for single-phase flow, the modeling strategy derives the filtered transport equations for phases where the filtered/resolved motion is separated from the sub-grid/unresolved contributions. The effect of unresolved structures is taken into account by an appropriate modeling of sub-grid contributions. Several models have been proposed for the sub-grid drag contribution (Igci et al., 2008; Parmentier et al., 2011). However, the sub-grid inter-species momentum exchange, as we have in poly-dispersed flow, has never been investigated. This phenomenon may have an important effect in the numerical simulations of chemical looping where fine particles entrain large particles by inter-species momentum transfer by collision. In the present work, we analyze highly resolved numerical simulation of binary particle mixture in a 3D periodic circulating fluidized bed to compare the contribution of the small-scale structures on the drag and inter-particle momentum exchange.

NOMENCLATURE

g	Gravitational acceleration (m/s^2)
P_k	Pressure of phase k (N/m^2)
d_p	Particle diameter (m)
C_d	Drag coefficient
$U_{k,i}$	Mean velocity of phase k (m/s)
m_p	Mass of particle p (kg)
n_p	Mean particle number density
e_c	Restitution coefficient
q_p^2	Agitation of the particle p (m^2/s^2)
Re_p	Particle Reynolds number
$Fr_{\Delta,q}$	Froude number of solid phase q

Greek letters

α_k	Volume fraction of phase k (-)
ρ_k	Density of phase k (kg/m^3)
τ_{fp}^F	Particle response time (s)
q_k^2	Agitation of phase k (m^2/s^2)
τ_{pq}^c	Collision timescale between p-q species (s)

Subscripts

g	Refers to the gas
$p2$	Refers to particles with small diameter
$p3$	Refers to particles with large diameter

MATHEMATICAL APPROACH

The modelling approach is based on the two-fluid model formalism involving mean separate transport equations of mass, momentum and fluctuating kinetic energy for each phase. Interactions between phases are coupled through interphase transfers. The transport equation for disperse phase fluctuations, q_p^2 developed in the frame of kinetic theory of granular media supplemented by the interstitial fluid effect and the interaction with the turbulence (Balzer et al., 1995; Gobin et al., 2003; Ciais et al., 2010), is resolved with taking into account inter-particle collisions between solid species on the dispersed phase hydrodynamic. In the present study we neglect the effect of gas turbulence.

The mass balance equation writes

$$\frac{\partial}{\partial t}(\alpha_k \rho_k) + \frac{\partial}{\partial x_j}(\alpha_k \rho_k U_{k,j}) = 0$$

where α_k is the k^{th} phase volume fraction, ρ_k the material density and $U_{k,j}$ the i^{th} component of the mean velocity. The volume fraction is related the mean density number n_k through the relation $n_k m_k = \alpha_k \rho_k$. The right-hand-side of the mass balance equation is equal to zero because no mass transfer takes place in the present study.

The mean momentum equation writes

$$\alpha_k \rho_k \left[\frac{\partial U_{k,i}}{\partial t} + U_{k,j}\frac{\partial U_{k,i}}{\partial x_j}\right] = -\alpha_k \frac{\partial P_g}{\partial x_i} + \alpha_k \rho_k g_i + \sum_{k'=g,p} I_{k'\to k,i} - \frac{\partial \Sigma_{k,ij}}{\partial x_j}$$

where P_g is the mean gas pressure, g_i the gravity, and $\Sigma_{k,ij}$ the effective stress tensor. The effective stress tensor has two contributions

$$\Sigma_{k,ij} = \langle u'_{k,i} u'_{k,i} \rangle + \Theta_{k,ij}$$

where $\langle u'_{k,i} u'_{k,i} \rangle$ is the kinetic stress tensor and $\Theta_{k,ij}$ the viscous stress tensor for the gas and the collisional stress tensor for the solid phase.

Gas-particle momentum transfers

The momentum transfers between the gas and the solid phase are only done by considering the drag and Archimedean forces. Then the gas-solid momentum exchange is given by:

$$I_{g\to p,i} = -\frac{\alpha_p \rho_p}{\tau_{fp}^F}(U_{p,i} - U_{g,i})$$

where $I_{g\to p,i} = -I_{p\to g,i}$. The particle relaxation τ_{fp}^F timescale is written in terms of the drag coefficient as

$$\frac{1}{\tau_{fp}^F} = \frac{3}{4}\frac{\rho_p}{\rho_g}\frac{\langle |v_r| \rangle}{d_p} C_d$$

with the drag coefficient given by the Wen & Yu correlation:

$$C_d = \begin{cases} \frac{24}{Re_p}\left[1 + 0.15 Re_p^{0.687}\right]\alpha_g^{-1.7} \\ 0.44\alpha_g^{-1.7} \end{cases}$$

The particle Reynolds number writes

$$Re_p = \frac{\alpha_g \rho_g \langle |v_r| \rangle}{\mu_g}$$

Particle-particle momentum transfers

As we consider polydisperse solid phase particle-particle momentum exchanges collisions between different particle species take place. Following Gourdel et al. (1998, 1999), Fede & Simonin (2005) and Zaichik et al. (2009) the momentum exchange by collision writes

$$I_{q\to p,i} = -\frac{m_p m_q}{m_p + m_q}\frac{1 + e_c}{2}\frac{n_p}{\tau_{pq}^c} H_1(z)(U_{p,i} - U_{q,i})$$

with e_c the normal restitution coefficient, τ_{pq}^c the p-q collision timescale and $H_1(z)$ a given function resulting from the analytical integration.

The collision timescale between two solid species writes

$$\frac{1}{\tau_{pq}^c} = 4 n_q g_0 \pi d_{pq}^2 H_0(z)\sqrt{\frac{2}{3\pi} q_r}$$

where $d_{pq} = (d_p + d_q)/2$ and $q_r = (q_p^2 + q_q^2)/2$ is the relative particle agitation where the correlation between colliding particle are neglected. The function $H_0(z)$ comes from the integration of the collision kernel. Such a function has an analytical expression (Gourdel et al., 1999) but for a practical use we employ the following approximation

$$H_0(z) = \sqrt{1 + \frac{\pi z}{4}}$$

where

$$z = \frac{(U_{p,i} - U_{q,i})^2}{8/3 q_r}$$

is a parameter quantifying ratio between the mean particle-particle velocity to the mean particle-particle relative agitation. For $z \to 0$ the inter-species collision are dominated by the relative agitation. In contrast, for $z \to +\infty$ the collision mechanism is controlled by the mean particle-particle relative velocity.

In the collision timescale, g_0 is the radial distribution function and takes into account the increase of collision frequency when the solid volume fraction is large. An expression has been proposed Mansoori et al. (1971) for polydisperse system. However their model as a finite value when the solid volume fraction reaches the maximum solid packing α_{max}. In 2007, Yang et al. proposed the following expression

$$g_0 = \left[1 - \frac{\alpha_s}{\alpha_{max}}\right]^{-2.5\alpha_{max}}$$

where $\alpha_s = \sum_{k=p} \alpha_k$ is the full solid volume fraction and $\alpha_{max} = 0.64$ the maximum solid packing for a random arrangement of particles.

Finally the inter-particle momentum transfer requires the knowledge of the function $H_1(z)$. As for $H_0(z)$ this function as an analytical expression (Zaichik et al., 2009) but for an easy implementation in CFD code we use the following approximation:

$$H_1(z) = \frac{8 + 3z}{6 + 3z}$$

Solid stress closure

The effective solid stress tensor may be rewritten as

$$\Sigma_{p,ij} = \left[P_p - \lambda_p \frac{\partial U_{p,m}}{\partial x_m}\right]\delta_{ij} - \mu_p\left[\frac{\partial U_{p,i}}{\partial x_j} + \frac{\partial U_{p,j}}{\partial x_i} - \frac{2}{3}\frac{\partial U_{p,m}}{\partial x_m}\delta_{ij}\right]$$

where the granular pressure is given by

$$P_p = \alpha_p \rho_p [1 + 2\hat{\alpha}_p g_0 (1 + e_c)]\frac{2}{3} q_p^2$$

and the bulk viscosity

$$\lambda_p = \alpha_p \rho_p \frac{4}{3}\hat{\alpha}_p g_0 (1 + e_c)\hat{d}_p \sqrt{\frac{2}{3\pi} q_p^2}$$

The solid viscosity $\mu_p = \alpha_p \rho_p \left(v_p^{kin} + v_p^{col}\right)$ is given in terms of the solid kinetic viscosity

$$v_p^{kin} = \frac{1}{2}\tau_{fp}^F \frac{2}{3} q_p^2 (1 + \hat{\alpha}_p g_0 \Phi_c) \times \left[1 + \frac{\tau_{fp}^F}{2}\frac{\sigma_c}{\hat{\tau}_p^c}\right]^{-1}$$

and the collisional viscosity

$$v_p^{col} = \frac{4}{5}\hat{\alpha}_p g_0 (1 + e_c)\left[v_p^{kin} + \hat{d}_p \sqrt{\frac{2}{3\pi} q_p^2}\right]$$

The model coefficients are

$$\Phi_c = \frac{2}{5}(1 + e_c)(3e_c - 1)$$

$$\sigma_c = \frac{1}{5}(1 + e_c)(3 - e_c)$$

The diameter $\hat{d}_p$, the solid volume fraction $\hat{\alpha}_p$ and collision timescale $\hat{\tau}_p^c$ are introduced for taking into account the effect of the polydispersion in the effective solid kinetic stress. These quantities write

$$\hat{\alpha}_p = \sum_q \alpha_q \frac{2m_q}{m_p + m_q}\left[\frac{d_{pq}}{d_q}\right]^3$$

$$\hat{d}_p = \frac{1}{\hat{\alpha}_p}\sum_q \alpha_q \frac{2m_q}{m_p + m_q}\frac{d_{pq}^4}{d_q^3}$$

$$\frac{1}{\hat{\tau}_p^c} = \sum_q \frac{2m_q}{m_p + m_q}\frac{1}{\tau_{pq}^c}$$

Turbulence model

The prediction of the solid agitation is done by solving an additional equation on q_p^2. This equation includes the friction of the particle with the gas assumed being laminar. Also the effects of inter-particle species are taken into account with the dissipation of q_p^2 by inelastic inter-species collision, the "thermal exchange" of agitation and the production of q_p^2 by the mean particle-particle slip velocity (Gourdel et al, 1998).

NUMERICAL SIMULATIONS OVERVIEW

Gas-particle flows were simulated in 3D Periodical Circulating Fluidized Bed (PCFB) by using the polydisperse Euler-Euler approach described in the previous section. The geometry, already used by Ozel et al. (2010), has a squared-section of 0.0275m and a length of 0.22m. The flow is driven in the opposite direction to the gravity by a uniform vertical pressure gradient contribution. In a similar way than Agrawal et al. (2001), the gas pressure is written as

$$P_g(x,t) = (z - z_0)\Delta P(t) + P_g'(x,t)$$

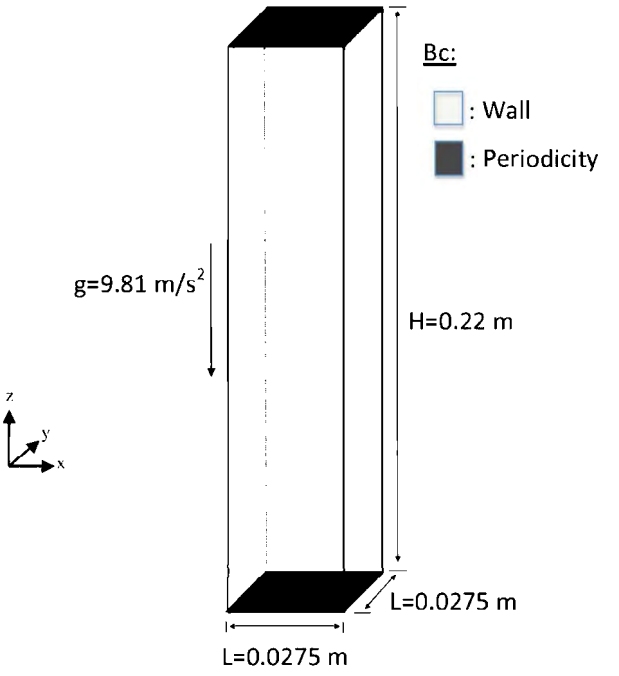

Figure 1: Geometry of the Periodical Circulating Fluidized Bed (PCFB).

The first term on the right-hand side represents the mean vertical pressure drop due to the total mass of two-phase mixture (hydrostatic part) and the momentum loss by the wall friction (no-slip boundary condition for the gas phase). The second term on the right-hand side is the computed gas pressure, which obeys the periodic boundary conditions.
Agrawal et al. (2001) tested three different choices of boundary condition for the particulate phase: no-slip, free-slip and partial slip (defined by a particle-wall coefficient of restitution and a specularity coefficient) and it was shown that the meso-scale structures occur with all types of boundary conditions. We chose to impose free-slip condition representing elastic bouncing of frictionless particles on a smooth wall whereas for the fluid no-slip boundary condition is imposed.

For the reference case, particles and gas material properties are summarised in Table 1.

Gas Phase	ρ_g	1.2 kg/m^3
	μ_g	1.8×10^{-5} Pa.s
Particles	ρ_{p2}	1500 kg/m^3
	d_{p2}	75 µm
Particles	ρ_{p3}	1500 kg/m^3
	d_{p3}	150 µm
	e_c	0.9
	Initial distribution $\alpha_{p,ini,2/3}$	0.05

Table 1: Solid and gas material properties.

Agrawal et al. (2001) stated that statistical quantities over the whole domain are strongly dependent on the mesh size and they become mesh-independent when mesh size is on the order of a few particle diameters. In this work, the mesh

refinement study is carried out to insure that the mesh resolution is sufficient and all spatial and temporal scales of solid and gas phases are captured. Figures 2 & 3 show the instantaneous particle volume fraction fields in the PCFB obtained by different mesh resolutions. As the mesh resolution increases, inhomogeneous structures are better resolved.

The mesh sizes and the computational grids are given in Table 2. As in previous studies (Agrawal et al., 2001; Ozel et al., 2010) the effect of the mesh size is analysed with respect to the Froude number Fr_{Δ}^{-1} defined as

$$Fr_{\Delta,p}^{-1} = \frac{\Delta}{\left(\tau_p^{St}\right)^2 |\mathbf{g}|}$$

with the Stoke's relaxation time τ_p^{St} given by

$$\tau_p^{St} = \frac{\rho_p}{\rho_g} \frac{d_p^2}{18 v_g}$$

And $|\mathbf{g}|$ is the norm of the gravity acceleration. The characteristic velocity $\tau_p^{St}|\mathbf{g}|$ is equal to $0.51m$ and the characteristic length scale $\left(\tau_p^{St}\right)^2|\mathbf{g}|$ is $0.0264\,m$ based on the larger particle properties. The length scale is approximately 10% of the column height that insures no effect of the periodic boundary condition on the results.

Number of cells	Mesh size ($10^{-3}\,m$)	Inverse Froude number Fr_{Δ}^{-1}
24×24×192	1.145	0.175 / 0.043
32×32×256	0.860	0.128 / 0.32
40×40×320	0.687	0.100 / 0.025
48×48×384	0.572	0.086 / 0.0215
64×64×512	0.430	0.064 / 0.016

Table 2: Computational grids and mesh sizes.

The numerical simulations have been carried out using an unsteady Eulerian multi-fluid approach implemented in the unstructured parallelized code NEPTUNE_CFD V1.08@Tlse. NEPTUNE_CFD is a multiphase flow software developed in the framework of the NEPTUNE project, financially supported by CEA (Commissariat à l'Energie Atomique), EDF (Electricité De France), IRSN (Institut de Radioprotection et de Sûreté Nucléaire) and AREVA-NP (Neau et al., 2010).

MESH INDEPENDENT RESULTS

To investigate the dynamic behaviour of particles in the PCFB, we define the following statistical quantities spatially averaged over the whole domain of volume V and in time over a period T. A time-averaged value $\overline{\langle Q \rangle}$ of spatial-averaged quantity $\langle Q \rangle$ is defined as

$$\overline{\langle Q \rangle} = \frac{1}{T}\int \frac{1}{V}\int Q(\mathbf{x},t)\,d\mathbf{x}dt$$

The time-spatial averaged solid mass flux along mean flow

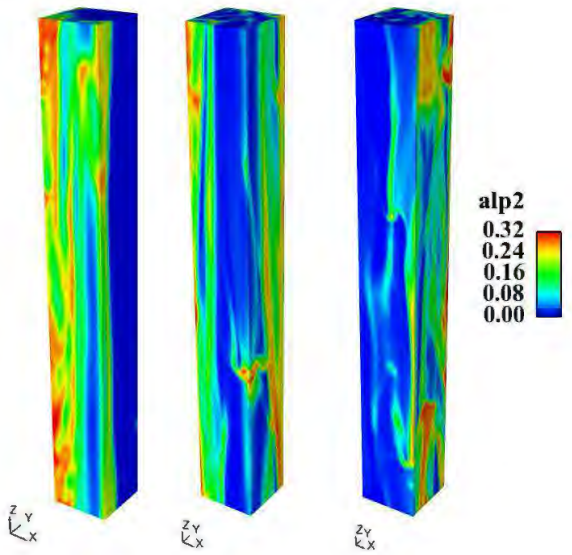

Figure 2: 3D view of instantaneous particle solid fraction of small particles 75 μm with respect to the mesh resolution; from de left to the right the mesh resolution increases.

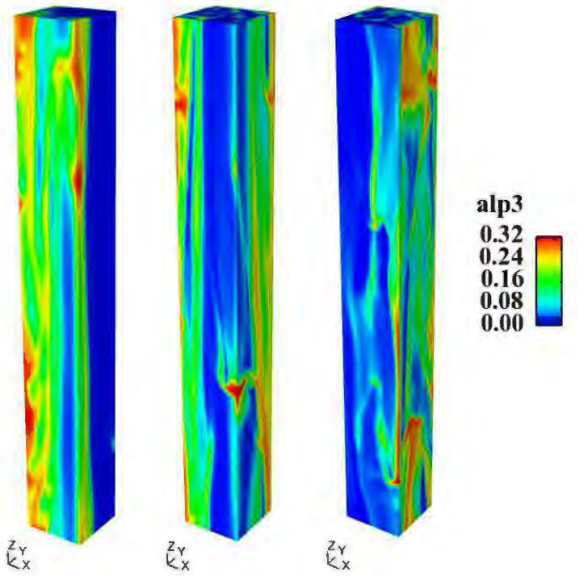

Figure 3: 3D view of instantaneous particle solid fraction of large particles 150 μm with respect to the mesh resolution; from de left to the right the mesh resolution increases.

direction is defined by for smallest particles:

$$\overline{G_{p2}} = \overline{\langle \alpha_{p2}\rho_{p2}U_{p2,z}\rangle}$$

and for largest particles

$$\overline{G_{p3}} = \overline{\langle \alpha_{p3}\rho_{p3}U_{p3,z}\rangle}$$

For the sake of simplicity, we refer to time-averaged of any spatial-averaged quantity as the average value of the quantity for the following sections. Each simulation was carried out for a long duration to ensure that a statistically stationary state reached (50 dimensionless physical time with the reference time scale set to the Stoke's relaxation time τ_p^{St} of larger particles. To obtain statistical quantities for all mesh resolutions, an equivalent number of realisations can be assured by a sample number that is calculated by the multiplication of number of cells with

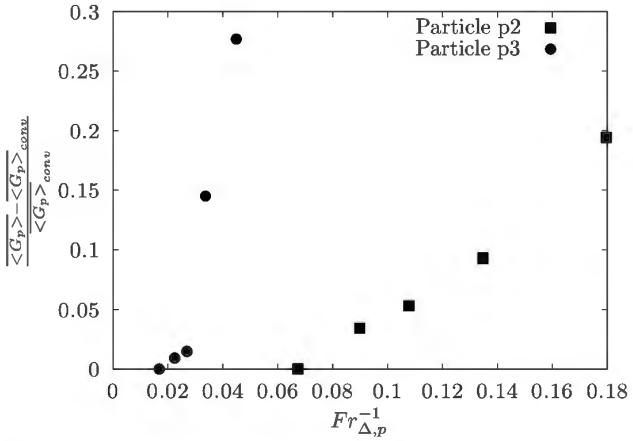

Figure 4: Influence of mesh size on the total volumetric mass flux $\overline{G_{p2}}$ and $\overline{G_{p3}}$. The subscript *conv* corresponds to the converged case, $Fr^{-1}_{\Delta,p2} = 0.064$.

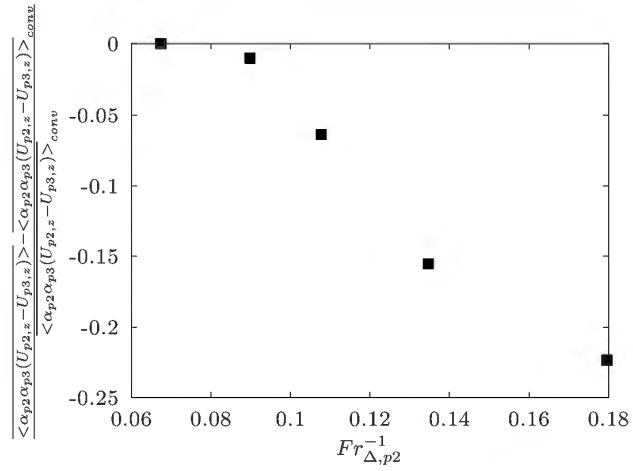

Figure 5: Influence of the mesh size, based on the smaller particle inverse Froude number, on the inter-particle relative velocity $\overline{\alpha_{p2}\alpha_{p3}(U_{p2,z} - U_{p3,z})}$. The subscript *conv* corresponds to the converged case, $Fr^{-1}_{\Delta,p2} = 0.064$.

dimensionless physical time. For highest mesh resolution, we computed statistics during another 50 dimensionless physical time. The total physical time for coarsest mesh simulation was yielded 20 times of the highest mesh resolution duration. After the flow reaches statistically stationary state, the averaged quantities are gathered. The mesh dependencies of total vertical solid mass flux with definition *conv* converged case are shown by Figure 4. The larger particle dependency on the mesh size is less sensitive than of the particles with smaller diameter. The larger particle reaches the converged result ($Fr^{-1}_{\Delta,p} < 0.04$) after few refinement studied. Ozel (2011) found the same Froude number for the mesh converged results for the A-type particles. In contrary, the converged results cannot be obtained for the smaller particles and further mesh refinement studies are necessary.

In this study, we present the effect of the mesh size resolution on the inter-particle momentum transfer due to collisions. Figure 5 shows the inter-particle relative velocity

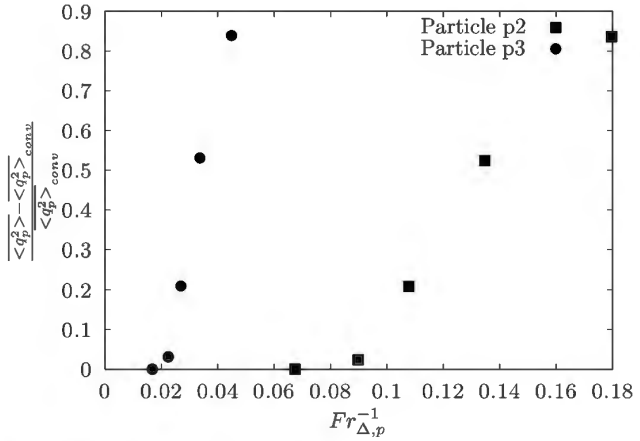

Figure 6: Influence of the mesh size on the particulate phases agitations. The subscript *conv* corresponds to the converged case, $Fr^{-1}_{\Delta,p2} = 0.064$.

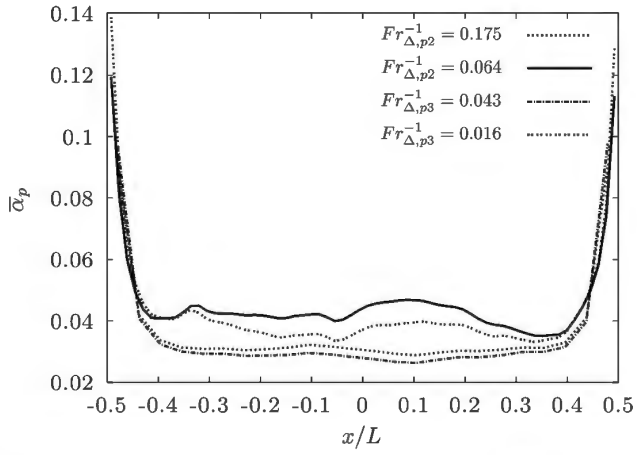

Figure 7: Radial profile of time-averaged solid volume fraction of the particulate phases $\alpha_{p,2}$ and $\alpha_{p,3}$ for two mesh resolutions: coarse (24×24×192, $Fr^{-1}_{\Delta,p2} = 0.175$ and $Fr^{-1}_{\Delta,p3} = 0.043$), fine (64×64×512, $Fr^{-1}_{\Delta,p2} = 0.043$ and $Fr^{-1}_{\Delta,p3} = 0.016$).

weighted by the particulate phase volume fractions for different mesh resolutions.

Figure 6 shows the mesh dependency of particulate phase agitations for the two particle species. It can be seen that the mesh independent results are obtained for both particulate phases. As compared with the solid mass flux evolution with respect to mesh size, the unresolved structures dramatically affect the particle agitations.

The radial distribution of time-averaged variables are shown by Figures 7-9 for two mesh resolutions: coarse (24x24x192, $Fr^{-1}_{\Delta,p2} = 0.175$ and $Fr^{-1}_{\Delta,p3} = 0.043$), fine (64x64x512, $Fr^{-1}_{\Delta,p2} = 0.043$ and $Fr^{-1}_{\Delta,p3} = 0.016$).

Figure 7 shows the time-averaged solid volume fraction for two resolutions. As expected we observe that the solid volume fraction is increasing in the near wall region. In contrast, at the centre of the geometry the profile of solid volume fraction is flattened. The case with the finer mesh depicts more fluctuation probably because more events are

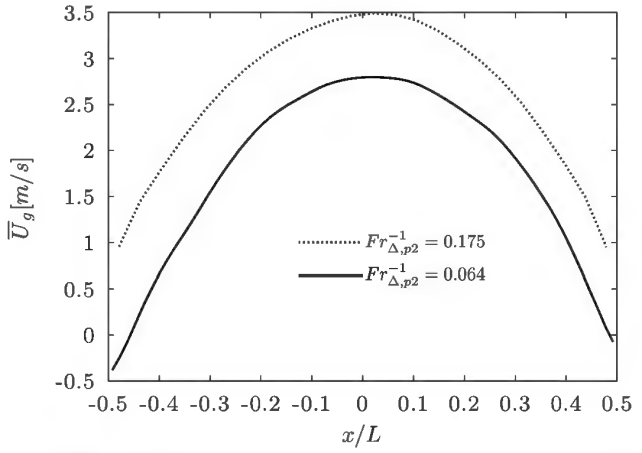

Figure 8: Radial profile of time-averaged vertical gas velocity for two mesh resolutions: coarse (24×24×192, $Fr^{-1}_{\Delta,p2} = 0.175$ and $Fr^{-1}_{\Delta,p3} = 0.043$), fine (64×64×512, $Fr^{-1}_{\Delta,p2} = 0.043$ and $Fr^{-1}_{\Delta,p3} = 0.016$).

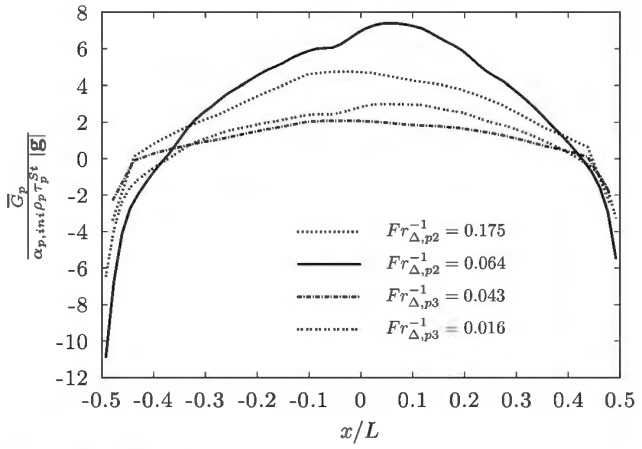

Figure 9: Radial profile of time-averaged total vertical solid mass flux of the particulate phases $\overline{G_{p2}}$ and $\overline{G_{p3}}$ for two mesh resolutions: coarse (24×24×192, $Fr^{-1}_{\Delta,p2} = 0.175$ and $Fr^{-1}_{\Delta,p3} = 0.043$), fine (64×64×512, $Fr^{-1}_{\Delta,p2} = 0.043$ and $Fr^{-1}_{\Delta,p3} = 0.016$).

necessary for the time-averaging procedure. By increasing mesh resolution, more particles are transported at the centre of the fluidized bed. As the solid mass is constant, it results that the solid volume fraction close to the walls is decreasing. As expected, the larger particles are less sensitive to mesh resolution.

The radial profiles of the mean gas vertical velocity showing by Figure 8 exhibit a strong effect of the mesh resolution because of the strong coupling between the solid phases and the gas. This trend was expected because the solid mass flux is modified by using a finer mesh.

Figure 9 presents the solid mass flux normalized by uniform distribution of solid falling down with the settling velocity $\tau_p^{St}|\mathbf{g}|$ for each solid phase. The core-annulus flow is obtained for coarse and finest mesh resolutions with and upward solid mass flux at the centre of the geometry and a downward solid mass flux near the walls.

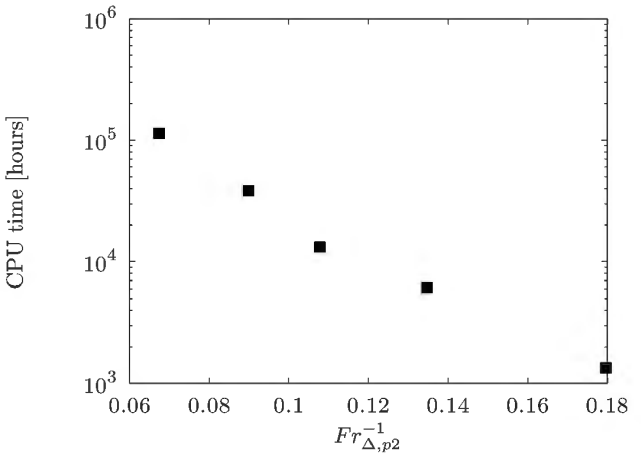

Figure 10: CPU times in hours required to simulate 1 second of the flow using the kinetic theory based Euler-Euler model.

The negative vertical solid mass flux decreases close to the wall with increasing mesh resolution due to the better prediction of flow mixing for the smaller particles.

The finest mesh resolution (64×64×512, $Fr^{-1}_{\Delta,p2} = 0.043$ and $Fr^{-1}_{\Delta,p3} = 0.016$) results are then used to construct a database of solid volume fractions, gas and particle velocities obtained on 10 times chosen every 2.5 Stoke's relaxation time during the statistically steady-state period of the simulation. This database is called as Euler-Euler DNS database and consists of 20 million of realizations of macroscopic variables. Then, we perform the volume averaging on these variables (see Ozel et al. 2010, Ozel, 2011).

Figure 10 shows the CPU times required to compute 1s of the flow. CPU time almost asymptotically increases as mesh resolution increases. The computational time is about 15 days on 128 processors (The simulations were performed on Bi-Xeon E5472 processors running at 3 Ghz) to reach statistically converged results for the case with the fine mesh resolution.

BUDGET ANALYSIS OF FILTERED PARTICULATE MOMENTUM EQUATION

Mesh independent results obtained in the previous section are then used for budget analyse of filtered particle momentum and agitation equations. The derivation of filtered Euler-Euler Two-phase model is given in Ozel (2011). Additional terms arising due to volume filtering require closure models. These budget analyses allow us to examine the contribution of additional terms coming from the filtering of the Euler-Euler set of equations. Several filter widths $\overline{\Delta}$ have been applied on the mesh-independent results.

We state the global equilibrium of fluidized particles between buoyancy force (gas pressure gradient), drag force, particulate stress, particle-particle momentum transfer due to collisions and gravity contributions.

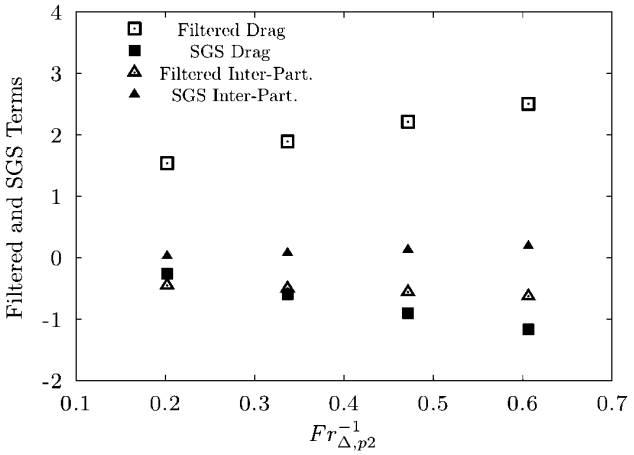

Figure 11: Filtered and sub-grid contributions drag and inter-particle collision forces normalised by the gravity term with respect to different inverse Froude numbers based on the filter width $\overline{\Delta}$ for small particles (75 μm).

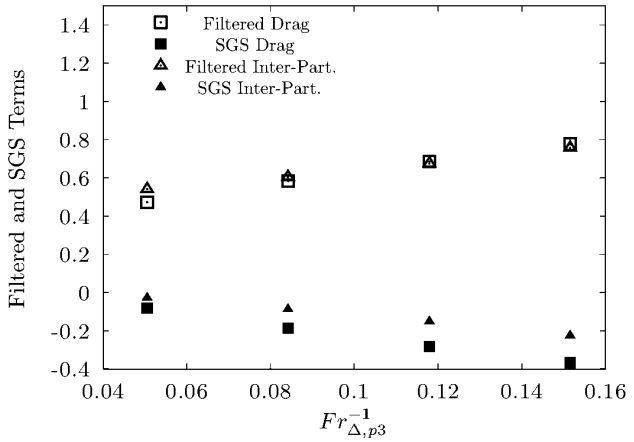

Figure 12: Filtered and sub-grid contributions drag and inter-particle collision forces normalised by the gravity term with respect to different inverse Froude numbers based on the filter width $\overline{\Delta}$ for large particles (150 μm).

The filtered and the sub-grid contributions of drag, gravity and inter-particle momentum terms normalised by the gravity term for inverse Froude numbers based on the filter width are shown by Figures 11 for small particles and by Figure 12 for large particles, respectively. We note that the sub-grid contributions of pressure correlation, kinetic and sub-grid stresses are negligible. The sub-grid contribution of drag force dramatically increases as filter width increases and it is consistent with the findings of Ozel et al. (2010) and Parmentier et al. (2012) where only one particulate phase was investigated. The drag term is overestimated, if the sub-grid contribution is not taken into account. The sub-grid contribution of inter-particle collision force shows the same trend as the sub-grid contribution of drag force for both particulate phases. We can note that if one performs simulation of poly-disperse gas-solid flows by using Euler-Euler two-fluid formalism on the relatively coarse mesh size respect to the small-scale structures, the collision frequency is underestimated.

CONCLUSIONS

Meso-scale structures are continuously formed in the circulating fluidized bed and they can be resolved through Eulerian approach by supplementing the kinetic theory of granular flows on high-resolution computational grid. However, simulations with mesh size larger than small-scale structure size cancel out these structures and this causes poor predictions of bed hydrodynamics. The cancellation of small-scale structures effect is investigated in details by Ozel et al. (2010), and Parmentier et al. (2012) for mono-dispersed gas-solid flow. In this study, we investigate effects of unresolved structures on resolved field for poly-dispersed flow, we first obtained mesh independent results of gas-solid in the 3D periodic circulating fluidized bed. We performed the filtering procedure on a given Euler-Euler model and obtained filtered particulate momentum equations.

Additional terms arising by the filtering procedure are investigated by budget analyses to determine their importance. It was yielded that meso-scale structures affect the flow characteristics profoundly. In particular, cancellation of these structures leads to overestimate the drag force between gas and particle phases and underestimate inter-particle collisions. For further studies, some models will be proposed to take into account sub-grid contribution of the inter-particle collision force.

ACKNOWLEDGEMENTS

This work was granted access to the HPC resources of CALMIP under the allocation P0111 (Calcul en Midi-Pyrénées).
This work was performed using HPC resources from GENCI-CINES (Grant 2012-x2012026012)

REFERENCES

Agrawal, K., Loezos, P., Syamlal, M., Sundaresan, S., 2001. The role of mesoscale structures in rapid gas–solid flows. Journal of Fluid Mechanics 445, 151–185.

Balzer, G., Boëlle, A., Simonin, O., Eulerian Gas-Solid Flow Modelling of Dense Fluidized Bed, FLUIDIZATION VIII, Proc. International Symposium of the Engineering Foundation, pp 409-418, 1995.

Balzer, G. Gas–solid flow modelling based on the kinetic theory of granular media: validation, applications and limitations Powder Technology, 2000, 113, 299 - 309

Ciais, V., Martin, R., Neau, H., Simonin, O. 3D Multiparticle Simulation of Volcanic Dome Collapse and Pyroclastic Flow: Application to 1984 and 1994 Events at Merapi Volcano 7th International Conference on Multiphase Flow, ICMF 2010, Tampa, FL, May 30 - June 4, 2007

Fede, P. & Simonin, O. Application of a perturbated two-Maxwellian approach for the modelling of kinetic stress transfer by collision in non-equilibrium binary mixture of inelastic particles 7th Int. Symp. on Gas-Particle Flows, 2005

Gourdel, C.; Simonin, O. & Brunier, E. Modelling and simulation of gas-solid turbulents flows with a binary mixture of particles Third International Conference on Multiphase Flow, 1998

Gourdel, C.; Simonin, O. & Brunier, E. Two-Maxwellian equilibrium distribution function for the modelling of a binary mixture of particles Proc. of the 6th Int. Conference on Circulating Fluidized Beds, Circulating Fluidized Bed Technology VI, 1999, 205-210

Igci, Y., Andrews, A.T., Sundaresan, S., Pannala, S., O'Brien, T., 2008. Filtered two-fluid models for fluidized gas-particle suspensions. AIChE Journal 54, 1431–1448.

Mansoori, G.; Carnahan, N.; Starling, K. & Leland, T. Equilibrium Thermodynamic Properties of the Mixture of Hard Sphere J. Chem. Phys., 1971, 54, 1523-1525

Neau, H.; Laviéville, J. & Simonin, O. NEPTUNE_CFD High Parallel Computing Performances for Particle-Laden Reactive Flows 7th International Conference on Multiphase Flow, ICMF 2010, Tampa, FL, May 30 - June 4, 2010

Ozel, A.; Parmentier, J.-F.; Simonin, O. & Fede, P. A Priori Test of Effective Drag Modeling for Filtered Two-Fluid Model Simulation of Circulating and Dense Gas-Solid Fluidized Beds 7th International Conference on Multiphase Flow, ICMF 2010, Tampa, FL, May 30 - June 4, 2010

Ozel, A.; Fede, P. & Simonin, O. A Posteriori Study of Filtered Euler-Euler Two-Phase Model Using a High Resolution Simulation of a 3-D Periodic Circulating Fluidized Bed AIChE Annual Meeting, 2012

Parmentier, J.-F., Simonin, O. & Delsart, O. A functional subgrid drift velocity model for filtered drag prediction in dense fluidized bed AIChE Journal, Wiley Subscription Services, Inc., A Wiley Company, 2011, 1-15

Simonin, O., Continuum Modelling of Dispersed Two-Phase Flows, in Combustion and Turbulence in Two-Phase Flows, Lecture Series 1996-02, von Karman Institute for Fluid Dynamics, Rhode Saint Genése (Belgium), 1996

Wen, Y. & Yu, Y. Mechanics of Fluidization Chemical Engineering Symposium Series, 1965, 62, 100-111

Yang, N., Patino, G., Fede, P., Simonin, O., Collision viscosity model assessment for dry granular flows composed of binary mixture of solid particles 6th International Conference on Multiphase Flow, ICMF 2007, Leipzig, Germany, 2007

Zaichik, L.; Fede, P.; Simonin, O. & Alipchenkov, V. Statistical models for predicting the effect of bidisperse particle collisions on particle velocities and stresses in homogeneous anisotropic turbulent flows International Journal of Multiphase Flow, 2009, 35, 868-878